JEE Journal of Ecological Engineering

*Journal of Ecological Engineering* 2024, 25(10), 189–208
https://doi.org/10.12911/22998993/192009
ISSN 2299–8993, License CC-BY 4.0

Received: 2024.07.12
Accepted: 2024.08.21
Published: 2024.09.01

# Semi-Automatic Monitoring of Grain Size and Shape Evolution of Fluvial Pebbles Along the Middle Inaouène River, Northern Morocco

Mohammed Lghamour[1*], Lhoucine Karrat[1], Vincenzo Picotti[2]

[1] Laboratory of Geosciences, Environments and Associated Resources, Earth Sciences Department, Faculty of science Dhar Mahraz, Sidi Mohamed Ben Abdellah University, 30003 Fez, Morocco

[2] Department of Earth Sciences, ETH Zürich, Sonneggstrasse, 5 8092 Zürich, Switzerland

* Corresponding author's e-mail: mohammed.lghamour@usmba.ac.ma

## ABSTRACT

Downstream pebble variability in river systems is assessed through various methods, with recent emphasis on efficient, time-saving semi-automatic processes involving photography and digital analysis. The Inaouène valley, however, lacked a comprehensive survey of its main channel using either manual or image-based methods. This study bridges this gap by combining both approaches to analyze the downstream evolution of surface pebbles' morphometric parameters along approximately 60 km of the Inaouène's middle reach. Our research focuses on two key aspects: grain size and particle shape. Results reveal a general downstream trend of size fining, increasing circularity and decreasing elongation, primarily attributed to abrasion and travel distance. Notably, this pattern is interrupted by localized variations associated with tributary inputs and sediment recycling processes. This study significantly contributes to the understanding of fluvial sediment dynamics in the Inaouène Valley. Its findings have broad implications, supporting ecological assessment and restoration efforts, while also informing decision-making in river engineering and management. By providing a comprehensive analysis of pebble characteristics and their downstream evolution, this research establishes a foundation for future geomorphological studies and practical applications in river system management.

**Keywords:** pebbles, size, shape, monitoring, semi-automatic, BASEGRAIN, downstream variability, geomorphology, Inaouène River, Morocco.

## INTRODUCTION

Gravels, commonly known as pebbles, are the coarser framework fraction of non-cohesive siliciclastic sedimentary rocks belonging hence to the rudite grain-size (GSi) class which universally have a minimum size of 2 mm. According to the particle size, gravels class include granules, pebbles, cobbles and boulders (Wentworth, 1922), it outlines also the sorting degree that varies from a very well sorted to an extremely poorly sorted gravel (Folk, 1974). In the same statistical way, the percentile d50 (or d30, d90) defines the dominant grains population in the case of an heterometric gravelly deposit, and thought to be a significant metric in related studies (e.g.,Parker et al., 1982). Gravel shape (GSh) is another physical property that is taken often into account for rivers studies, it characterizes "The external geometrical expression" of this particle (Blott and Pye, 2008).

These reworked (epiclastic) rock fragments are initially derived from the hinterland basin by surficial terrigenous process such as weathering and mechanical erosion, transported and deposited then either in a proximal or a distal environment through gravity or fluid-flow dynamics. The latter ones play a key role in a fluvial setting; indeed, alluvial rivers yield consistently with the dominant geomorphic drivers, between 90% in mountainous areas, and less than 10% of gravels in more gentle transects (Bunte and Abt, 2001), and tend to settle them transitionally in their beds. Thereby, Fluvial gravels are globally ubiquitous and exist even on Mars (Jerolmack, 2013; Szabó et al., 2015).

In the gravelly alluvial rivers or reaches, riverbeds and channel bars provide the space for gravels to be accommodated. Because of its high sensitivity, this axial channel belt records most of the hydrodynamic events and oscillations, whom remain printed on the subsurface sedimentary archive as well as on the river morphology. The same component offers a favorable biotope substrate for several continental aquatic species responding hence similarly to these external forces (eg., Crosa et al., 2010; Geist and Auerswald, 2007; Hauer, 2015; Hauer et al., 2015, 2013; Kondolf and Wolman, 1993; Pulg et al., 2013; Sutherland et al., 2002).

As a geomorphic and physical environmental component of the landscape, the Inaouène riverbed or (stream) still a poorly studied area, The main related works were interested in the hydraulic modeling and the assessment of water quality (e.g.,Laaraj et al., 2022, 2020; Naoura et al., 2012). Moreover, based on the GIS applications, the attention was paid also to the correlation between sediments fluxes and the erosional physiographic characteristics of the Inaouène's watershed (Benzougagh et al., 2021, 2020; Brahim et al., 2020, 2017; Garouani and Tribak, 2006; Lahsaini et al., 2018; Marouane et al., 2021; Sibari et al., 2018; Snoussi et al., 2002). Therefore, assessments of the main channel's physical aspects is required to fill this geomorphological wide gap.

The present paper delivers results of a spatial systematic high-resolution monitoring of the recent fluvial (alluvial) gravels laying at the main channel bed, from the up to the downstream of the middle Inaouène river. We conducted an accurate modern field longitudinal investigation of the caliber and shape distribution of this build-up, projected then to various multidisciplinary applications ranging from decision making in environmental management to fluvial geomorphology.

## GEOGRAPHICAL AND GEOLOGICAL SETTING

Situated in central north of Morocco, The Inaouène main River is an inter-mountainous tributary stream that runs westward crossing the north of Taza city following a sub-equatorial trend, and joins the larger river of Sebou to the northeast of Fez city (Lat 34°13' 20.45"N; Long 4°54'34.43"W; 129 m a.s.l), reaching then a total length of 228 km. Its tributaries network extends over an area of 5184 km$^2$ covering the relatively moderate prerifian relief to the north, and the last piedmonts of the Middle Atlas range to the southern part, there where the elevation achieves its highest peak (up to 1600 m a.s.l). The reach of interest is located in the middle valley of Inaouène, between Oued Amlil village and the lake reservoir of Driss I dam (Figure 1b).

The Oued Inaouène main channel shows clear evidences of a meandering and sometimes wandering system, running on a mixed generally soft but locally resistant bedrock. A previous ecological investigation reveals the high abondance of riparian vegetation inside and alongside the Inaouène channel, the most dominant plants species

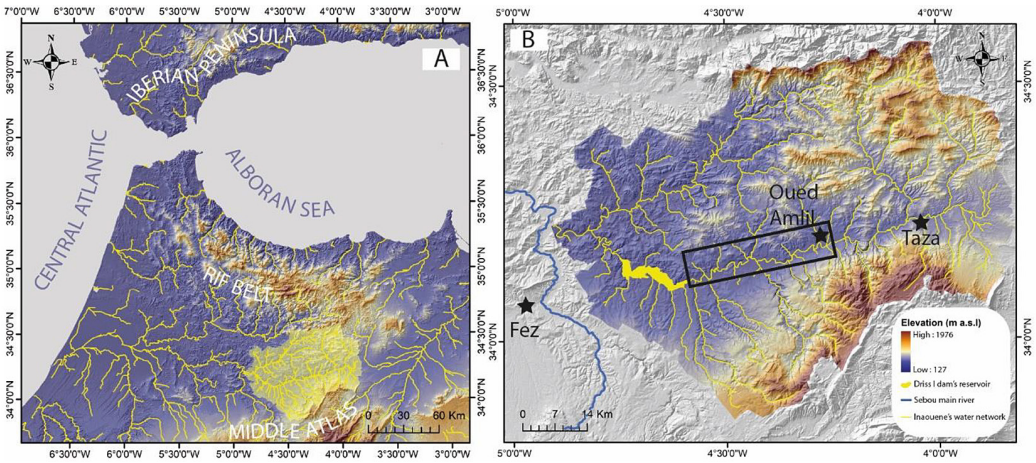


**Figure 1.** Location of the study area, (a) geographical setting of the Inaouène River catchement area within northern Morocco; the yellow golden frame indicates its shape and location between the Middle Atlas and the Rif ranges, (b) shape and relief of the studied river catchement area; the black frame locates the middle reach of the Inaouène Valley (see Figure 3)

there are Tamarix gallica, Tamarix africana and Arundo donax (Libiad et al., 2012).

Inside the Inaouène's catchment area, lithological formations are mainly composed by middle Miocene and cretaceous marls and sandstones, belonging to the Prerif chaotic units to the north and to the foreland basin alongside the median corridor. Liasic limestones and dolomitic rocks are dominants in the middle atlas land which also hosts a large outcrop of Paleozoic basement called the Tazekka massif (Michard et al., 2010). This NE-SW oriented bloc is primarily formed by schistose series and other metamorphic rocks, with subsidiary magmatic and sedimentary units (Figure 2).

## MATERIAL AND METHODS

The survey approach is primarily based on the field examination of the fluvial gravel's physical patterns, from the upstream to the downstream of the Inaouène riverbed. Sampling points, or in other words, the studied stations were previously fixed according to the discussed aims. Achieving these aims was hence ensured by the use of some numerical and statistical processing of the collected data.

### Determination of sampling locations (sampling strategy)

Selection of site and time represents the first step for bed-material sampling (Kellerhals and Bray, 1971); accordingly, our work is interested on the axial main channel belt of the Inouaène River Valley, we essentially investigated here the apparent channel bars and emerged riverbeds deposits. Generally, the best geomorphic riverine portions that provide a clear overview of the bed-material are the channel-neighboring and in-channel riffles, the reason is linked indirectly to the access facility because of the water's table shallowness, and directly to the focus of disposition in these areas (Galia, 2017). Indeed, in a sinuous setting, bank attached bars extend into riffles (Church and Jones, 1982) and provide a storage space there. Moreover, riffles tend to host the most uniform hydraulics, resulting in less spatial variability in particle size, they offer consequently an optimal location for gravels examination (Bunte and Abt, 2001). For the investigation period, we preferred to conduct the study in spring 2023, after the last high-water event of the winter flood.

In this way, we choose systematically 12 sampling points (G1, G2…. G12) inside the channel

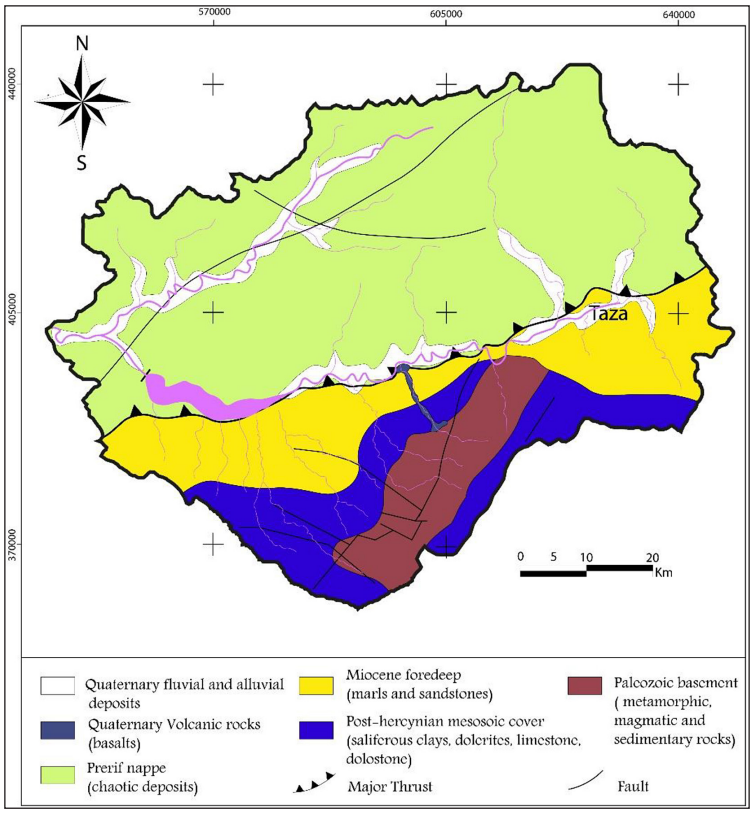


**Figure 2.** A Simplified geological map of the Inaouène River catchment area after (after Morel 1992; Suter 1980)

belt of the middle Inaouène Valley, with an average real spacing of 5 km. we gathered then the necessary data from each station (G) accordingly with the previous criteria in order to monitor the evolution of these gravels (Figures 3–5).

## Examination of the gravelly bed-material

This step consists of the assessment of two important physical features related to the modern gravelly load of the Inaouène: The grain size distribution (GSiD) (i), and the grain-shape distribution (GShD) (ii) of these gravels. It is an attempt to derive a total-system pattern through a high-resolution quantitative approach that is interested in nesting sub-units' information.

### *Field work*

Traditionally, two standard approaches have been used to examine the GSiD (i) of unlithified clastic sediments involving laboratory sieving, typically applied for finer fractions (Folk, 1974; Ingram, 1971), or in-situ methods such as the Wolman pebble count following a line (Fehr, 1987; Wohl et al., 1996) or a dimensioned implemented grid-by-number (Kellerhals and Bray, 1971; Wolman, 1954), employed especially for coarser particles. To obtain a valid count, this manual field examination requires the measurement; by caliper or rule, of the intermediate diameter (Di) (b-axis in literature) for at least 100 particles, it's considered hence, to be analogous to volumetric sampling methods (Bunte and Abt, 2001). For this reason, the pebble count technic is widely applied in fluvial geomorphology even for modern works (eg., Baynes et al., 2020; D'Arcy et al., 2017; Guerit et al., 2018, 2014; Watkins et al., 2020). However, both approaches remain challenging and have some serious issues, namely, classical sieving requires relevant efforts and resources, while manual pebble counts are time-consuming, inaccurate, destructive and prone to human subjectivity (Daniels and McCusker, 2010; Eaton et al., 2019; Green, 2003; Purinton and Bookhagen, 2021; Rice and Church, 1996; Steer et al., 2022; Wolcott and Church, 1991).

In a similar manner, manual morphological analyses; also known as sedimentary particles shape evaluation ((GShD)(ii)), provide a significate amount of data applicable to rivers' dynamics (Krumbein, 1941; Müller, 1967; Powers, 1953; Wadell, 1935, 1933). However, these classical routines require several measurements for each particle, which can be time-consuming and resource-intensive when dealing with a batch of clasts.

Since the 1970s, computerized digital images have been recognized as high performant tools for geological manipulations (Condit and Chavez, 1979), correspondingly, photographs have been used for manual digitalization ("photo sieving"), providing alternative and more suitable grain-sizing options for the examination of the pebbles' GSiD (eg., Ibbeken and Schleyer, 1986; Kellerhals and Bray, 1971). Recently, this approach acquires more technical advances, indeed, Digital imaging inspections are frequently applied following the wide commercialization of handheld and Unmanned Aerial vehicle (UAV) high quality cameras (eg., Detert et al., 2018; Graham et al., 2005; Kozakiewicz, 2013; Maerz et al., 1996; Purinton and Bookhagen, 2021, 2021; Soloy et al., 2020; Stähly et al., 2017; Steer et al., 2022; Strom et al., 2010). The same reasons stand behind the proliferation of image-based GShD studies (e.g.,

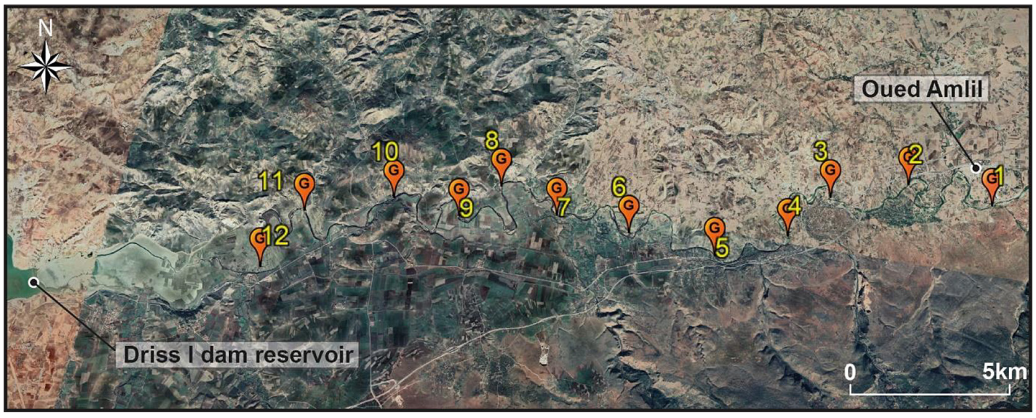


**Figure 3.** A satellite image (Google Earth) of the sampling stations (G1, G2… G12) of the bed-gravelly material along the middle Inaouène River


**Figure 4.** Overviews of the studied stations from G1 to G6. The long white arrows indicate the river-flow direction, while the short arrows exhibit the scaling tools (yellow arrows: a 40 cm long backpack; black arrows: a 30 cm long ruler)

Al-Rousan et al., 2007; Charpentier et al., 2013; Roussillon et al., 2009; Sun et al., 2012; Tafesse et al., 2012; Tunwal et al., 2020; Vangla et al., 2017; Yang et al., 2021).

Within our field investigation, two successive steps were conducted in each station (G), the first one consists of capturing images of the gravel bed, in this case, a serie of top-viewed adjacent photos was taken following a half cross-sectional line. We use a smartphone (Sony Xperia XZ premium) hand-held camera, its Exmor RS sensor is called Sony IMX400 and have a resolution of 19 Megapixels, and a pixel size of 1.22 µm. The heigh of each capture varies between 1.5 and 2 m, but generally, all the photos were recorded from a head-position heigh. To obtain the best possible results afterward, an optimal practice was applied while photographing (Detert and Weitbrecht, 2013), the essential condition here is to ensure the highest possible quality of the taken pictures. To do so, we avoided the perspective distortion by the perpendicular positioning of the camera to the bed, as well as by using one single scale. Furthermore, in order to keep away from any image processing issues, it was necessary to minimize the amount of cast shadowing as much as possible, and to take photos from non-totally or partially wetted parts of the bed, while avoiding also the other non-lithic particles such as plants, human made objects, snow, etc.

The next step involves the manual sampling of a considerable amount of gravel material,

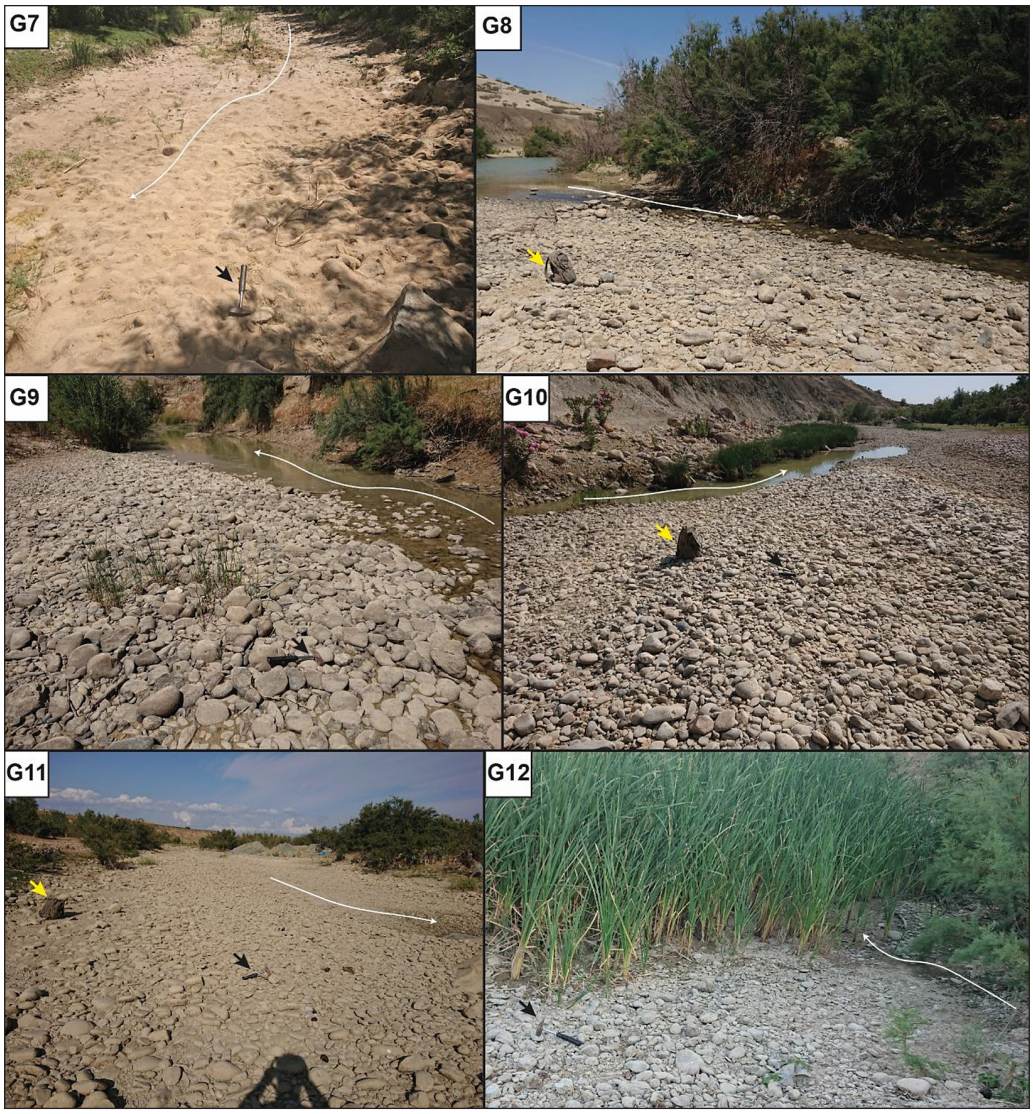


**Figure 5.** Overviews of the studied stations from G7 to G12. The long white arrows indicate the river-flow direction, while the short arrows exhibit the scaling tools (yellow arrows: a 40 cm long backpack; black arrows: a 30 cm long hammer)

aiming hence one important goal: a supportive manual measurement for the GSiD and the GShD numerically derived results.

### *Image-based processing and digital computation of results*

After the photos collection, the processing stage focused on the digital identification of gravels in these images, then, the extraction of information followed by the statistical computation of the essential metrics related to the GSiD and GShD of the Inaouène river-bed.

For this purpose, we adapted an object detection method that was applied firstly by Graham et al. (2005a, 2005b), technically known as "The Digital Gravelometer". This method was further developed and enhanced by Detert and Weitbrecht (2012) to address some technical challenging issues. The former process briefly aims to recognize the gravel particles and to statistically describe the geometry of these photographed gravels. In details, this MATLAB-based automated methodology relies on six steps and was applied exclusively for the GSiD; the first three steps include the interstices detection using different filters, while the fourth step focuses on the individual isolation of grains (the watershed separation). Following, the fifth operation consists of transforming the grains views into elliptical forms with proper geometrical indices including the long axis (a-axis), the intermediate one (b-axis), area, perimeter and direction. Finally, "a GSiD Digital

image analysis" is performed based on a "transfer to quasi-sieve analysis". The whole operation is facilitated by a Graphical User Interface (GUI), which itself evolved lately to become a stand-alone software tool called BASEGRAIN (Detert and Weitbrecht, 2013).

In our study, we easily uploaded the captured photos of the middle Inaouène bed's gravels to a PC-installed BASGRAIN software, then, the images processing was conducted to automatically obtain the GSiD results (b-axis length) (Figure 6). We choose this tool because of its simplicity provided by its user-friendly interface, in addition to the related support resources availability. Moreover, the BASEGRAIN output is fruitful, accurate and can be applied in a wide range of studies.

Accordingly, we exploited the deliverable of BAISGRAIN to assess, for the first time, the GShD of a riverbed gravel. The long a-axis and intermediate b-axis lengths were statistically compiled in order to quantitatively describe two planar (2D) shape parameters (Figure 7); the elongation and the circularity of the Gravely bed-material.

The elongation index (El) is thought to be one of the most important aspects of particle forms

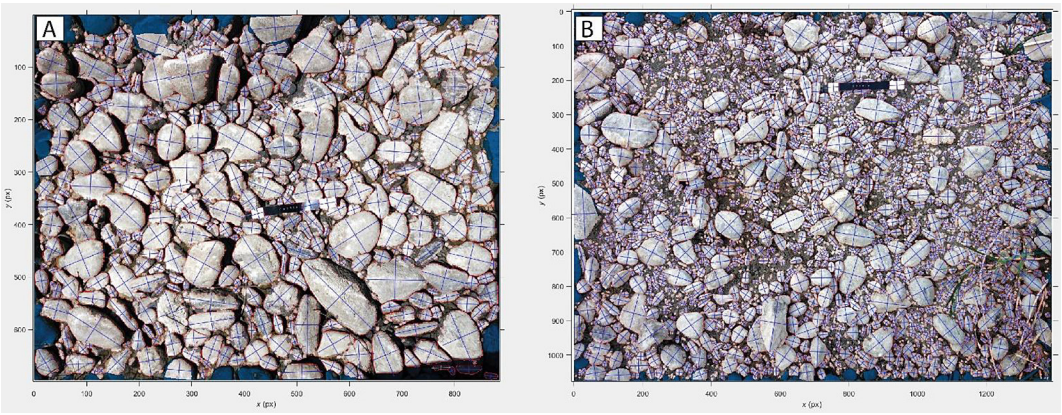


**Figure 6.** Examples of BASGRAIN's interface while processing the images captured from channel bed in stations G9 (A) and G12 (B). note the presence of two perpendicular bleu lines upon each element, they represent the extracted dimensions of long-axis (a) and intermediate-axis (b) of gravels after scaling (black and white ruler is 30 cm long)

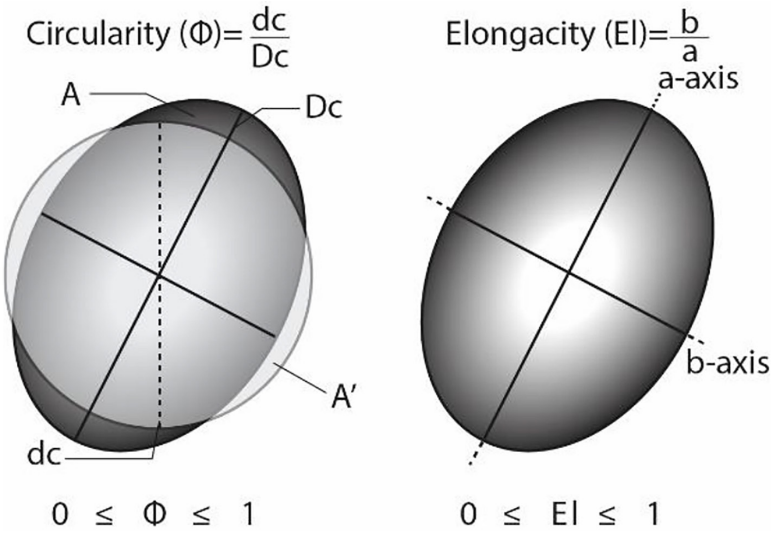


**Figure 7.** Shape parameters of the 2D projection of a gravel grain (represented by the graded black ellipse). The transparent greyish circle refers to the equivalent circle with the same area (A') as the particle ellipse (A): A'= A. The circularity ratio is calculated according to (Wadell, 1935), dc identifies the diameter of the equivalent circle, while Dc determines the ellipse major axis, also noted a-axis in the right illustration, where the b-axis displays the intermediate axis

(Blott and Pye, 2008), it represents the mathematical response to how long is a particle question, and can be inferred through the calculation of the b/a ratio for each particle (Köster and Leser, 1967; Krumbein, 1941). The yielded values range from zero indicating hence an extremely long particle, to one suggesting that the particle is non-elongate which means that is have an equant form. Afterward, frequency diagrams were established and an average elongation value is calculated for every spot. A verbal suggested classification is applied then accordingly with Blott and Pye (2008).

The circularity ($\Phi$) as it was defined by Wadell (1933) express the ratio between the circumference of a circle that have an equivalent area with the analyzed ellipse (i.e., the particle silhouette), and the real perimeter of this ellipse. One may view this parameter as an equivalent expression of grain sphericity in a two-dimensional plane (Blott and Pye, 2008; Roussillon et al., 2009; Wadell, 1935). We used here another derived formula which put into ratio the particle's analogue diameter ($d_c$) and the ellipse a-axis ($D_c$) (Soloy et al., 2020; Wadell, 1935), the inferred values vary between zero for a perfectly non-circular gravel, and one in case of a perfectly circular coarse clast. Finally, in a similar way to the previous elongation analysis, we proceed with the following statistical treatments to complete the related characterization of this parameter.

## RESULTS

In this section, we will present the various findings, including the correlation between image-based and manual measurements, as well as the evolution of GSiD and GShD.

### Bridging manual and BASEGRAIN assessments

Obviously, the BASEGRAIN's accuracy was tested in many occasions (Detert and Weitbrecht, 2013, 2012; Stähly et al., 2017), where it was suggested that gravel-bed dimensions obtained through BASEGRAIN numerical examen can be readily compared to grain sizes derived using manual methods. However, we verify herein the implication of these combination in the studied field, through the use of linear correlation between the value of the maximum manually-assessed intermediate axe ($b_{max}$), and the maximum numerically-derived intermediate axe in each station. Similarly, the second linear correlation is established between the average of shorter and longer manually-assessed intermediate axe ($b_{avg}$) and its homologue for image-based results. We aim by this statistical analysis to support and valid the reliability of our subsequent GSiD and GShD numerically-inferred evolution (Figure 8).

The above graphs show a downstream strong positive correlation between manually and numerically assessed intermediate axes, r pearson reaches 0.75 and 0.84 for $b_{max}$ and $b_{avg}$ correlations respectively. This means a high degree of positive association in our case, between the manual and image-based results, therefore, both of them vary proportionally in the same way.

### Grain-size distribution results

The Table 1 is established based on the metadata inferred from each station's image analysis, it exhibits the evolution and variation of some parameters according to the stations and the scale of the captured image. The scale here seems to

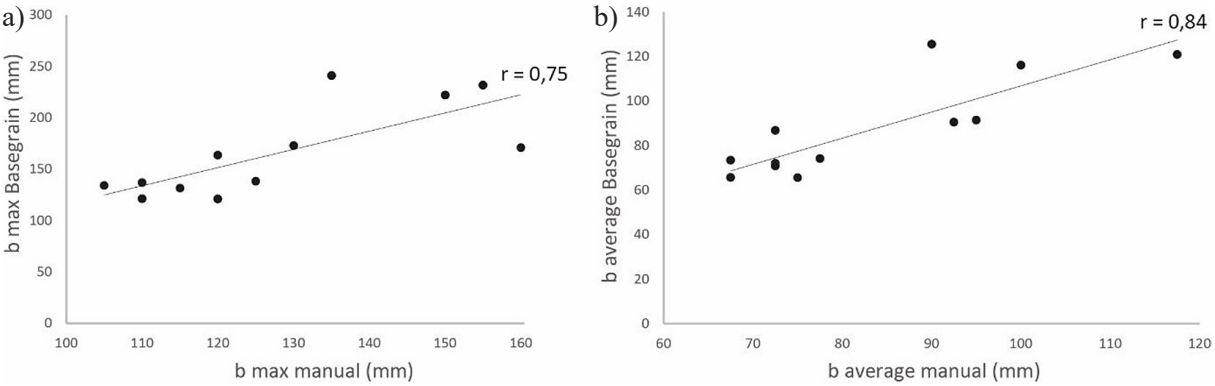


**Figure 8.** Linear correlation between manually-assessed and numerically-inferred maximum intermediate axes (a) and average intermediate axes (b) alongside the 12 studied locations

**Table 1.** Metadata inferred from BASGRAIN-image analysis for each station (G1 to G12)

| Station | Scale (mm/px) | Void (%) | Non-void (%) | Full grains (%) | Full grains | Measurements | b-max (mm) |
|---|---|---|---|---|---|---|---|
| G1 | 1.1143 | 27.9 | 72.1 | 75.3 | 2061 | 866 | 241.1 |
| G2 | 1.1976 | 40.1 | 59.9 | 60.8 | 2138 | 1078 | 231.9 |
| G3 | 1.2781 | 22.2 | 77.8 | 71.6 | 1756 | 1214 | 173.0 |
| G4 | 1.2615 | 24.0 | 76.0 | 73.5 | 1542 | 965 | 222.2 |
| G5 | 1.8045 | 31.0 | 69.0 | 63.6 | 1561 | 1369 | 134.1 |
| G6 | 1.7132 | 29.4 | 70.6 | 68.8 | 1043 | 917 | 121.1 |
| G7 | 1.8074 | 28.1 | 71.9 | 65.7 | 1050 | 918 | 138.4 |
| G8 | 1.7925 | 27.9 | 72.1 | 67.0 | 1006 | 886 | 171.0 |
| G9 | 1.5595 | 24.8 | 75.2 | 71.2 | 688 | 509 | 131.7 |
| G10 | 1.7730 | 34.6 | 65.4 | 64.3 | 1095 | 980 | 136.9 |
| G11 | 1.6947 | 46.4 | 53.6 | 56.0 | 1065 | 880 | 163.6 |
| G12 | 1.1451 | 28.3 | 71.7 | 69.0 | 2971 | 1791 | 121.3 |

be variable because of the conditions of images capture. The most important data in this table is the b-max measurement which shows a clear evolution well described in Figure 10.

The grain-size distribution analysis reveals a predominant presence of pebble-sized grains (with a d50 ranging between 25 and 60 mm) along the middle section of the Inaouène River. However, there is notable variation between different sections of the river. Upstream, particularly at the first six stations, there is a higher abundance of coarser clasts compared to the downstream

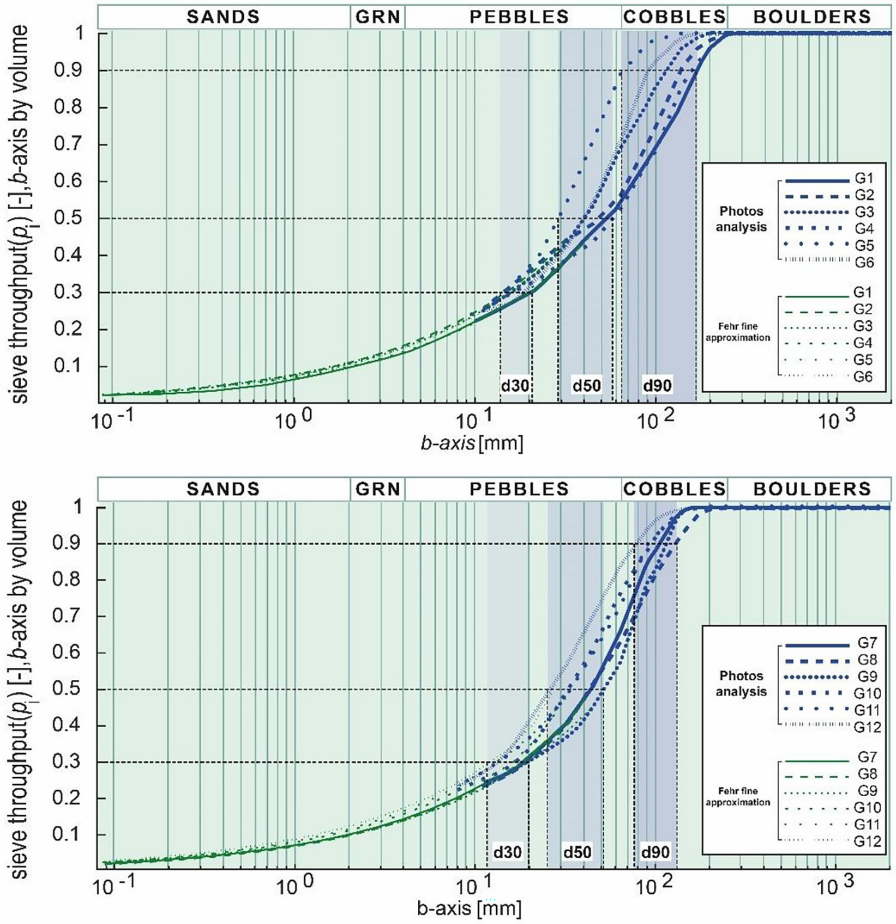


**Figure 9.** Grain size plots of the clasts derived from different studied stations

stations (G7 to G12). This is evidenced by a general decrease in d30, d50, and d90 limits and intervals downstream (Figure 9).

The downstream variability curves of the grain size parameters exhibit distinct patterns. For example, the d30 curve remains relatively stable across all stations. The d50 curve shows a slight decrease and increase from station G1 to G4, followed by another slight decrease at station G5, then gradually increases up to station G9, where it experiences a slow decrease towards the last downstream station. Both the d90 and b-max curves highlight a general decrease in the studied sizes: From station G1 to G12, the d90/b-max decreases from around 160/250 mm to approximately 60/130 mm. Furthermore, these last two parameters illustrate at least three cycles of downstream variations, characterized by periods of decrease followed by increase. For example, the b-max curve exhibits a first cycle from G1 to G4, a second from G4 to G8, a third from G8 to G11, and a half cycle (decrease) from G11 to G12. Similarly, the d90 curve reflects a first cycle from G1 to G4, a second from G4 to G8, and a half cycle from G8 to G12 (Figure 10).

The downstream evolution of the sorting index follows a cyclic pattern, as depicted by the associated curve. It initially decreases from station G1 to G2, followed by a complete increase-decrease cycle from G2 to G5, with a peak observed at G4. A similar cycle begins at G5 and culminates in peaks at G8 and G9. This second cycle reaches its minimal value at the last station, G12. Overall, this evolution generally shows a positive correlation with the b-max curve. For instance, the first maximum in the b-max curve aligns with the first maximum in the sorting index (SI) curve at G1, while the subsequent b-max peak corresponds to the second peak of SI at G4. A similar alignment occurs at G8, where the SI curve displays another maximal value. However, exceptions are observed at G11 and G9, where peaks in the b-max and SI curves respectively do not demonstrate this positive correlation between these two parameters. In overall, for the sorting character, the results from all the stations from G1 to G9 fall-out in the domain of very poorly sorted clast, while stations from G10 to G12 have more sorted clasts (Figure 11).

## Grain-shape distribution results

Shape is a critical characteristic defining the morphometry of a clast. As mentioned earlier, this morphometry in a 2D plane is evaluated through two key parameters: Circularity and Elongation. The distribution of the related indexes was tracked along the Inaouène channel, with the results elaborated below. Before we delve into the details, it's worth noting that the elongation index (Ei) is inversely proportional to elongation, while the circularity index tends to be directly proportional to circularity.

The analysis of Ei frequencies across multiple stations reveals diverse findings (Figure 12). Broadly, the maximum Ei value across all stations is approximately 1, indicating some pebbles that lack elongation, while the minimum varies from 0.14 (suggesting extreme elongation) at G2 to 0.27 (indicating high elongation) at G10. Mean values

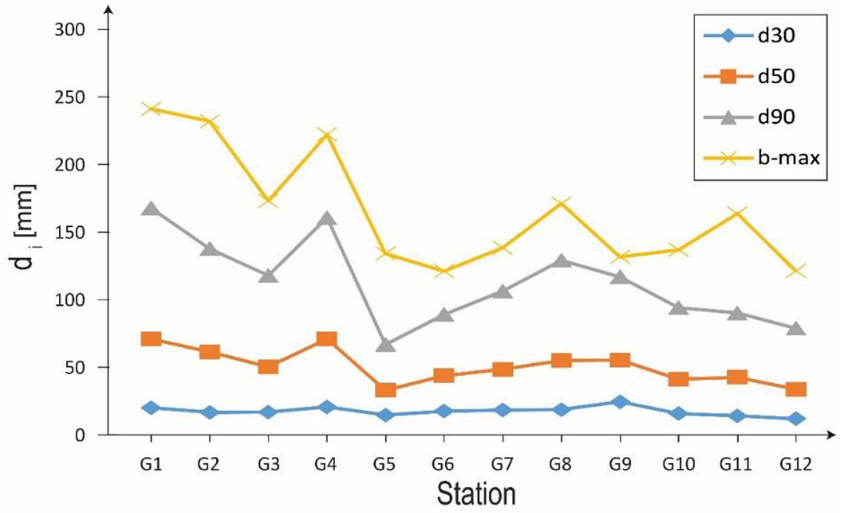


**Figure 10.** Downstream variability of the grain-size parameters

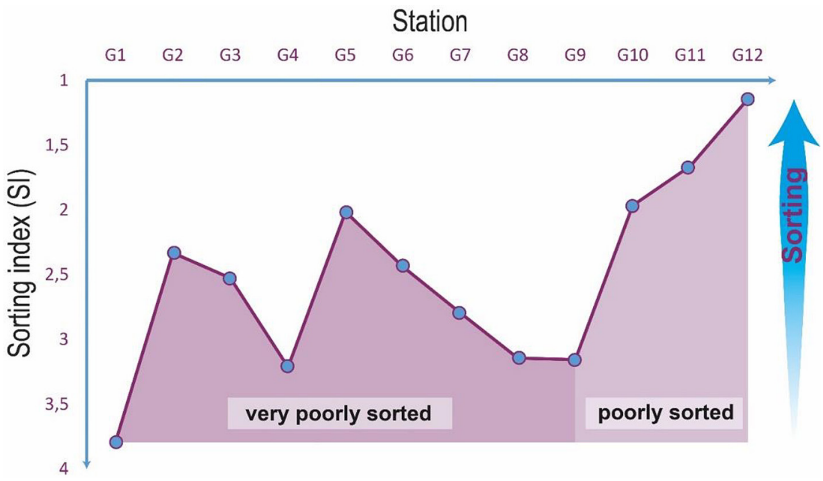


**Figure 11.** The downstream evolution of the sorting index evolution across the studied stations

range from 0.64 at G1 to 0.71 at G5, G7, and G11, all falling within the category of slightly elongated pebbles. The average of these mean values is approximately 0.69, suggesting that the typical class of pebbles in the middle Inaouène River is slightly elongated. The highest bars representing maximum values of class frequencies indicate that all stations predominantly contain slightly elongated pebbles (Ei: 0.6–0.8). Conversely, minimal or zero values of these frequencies suggest

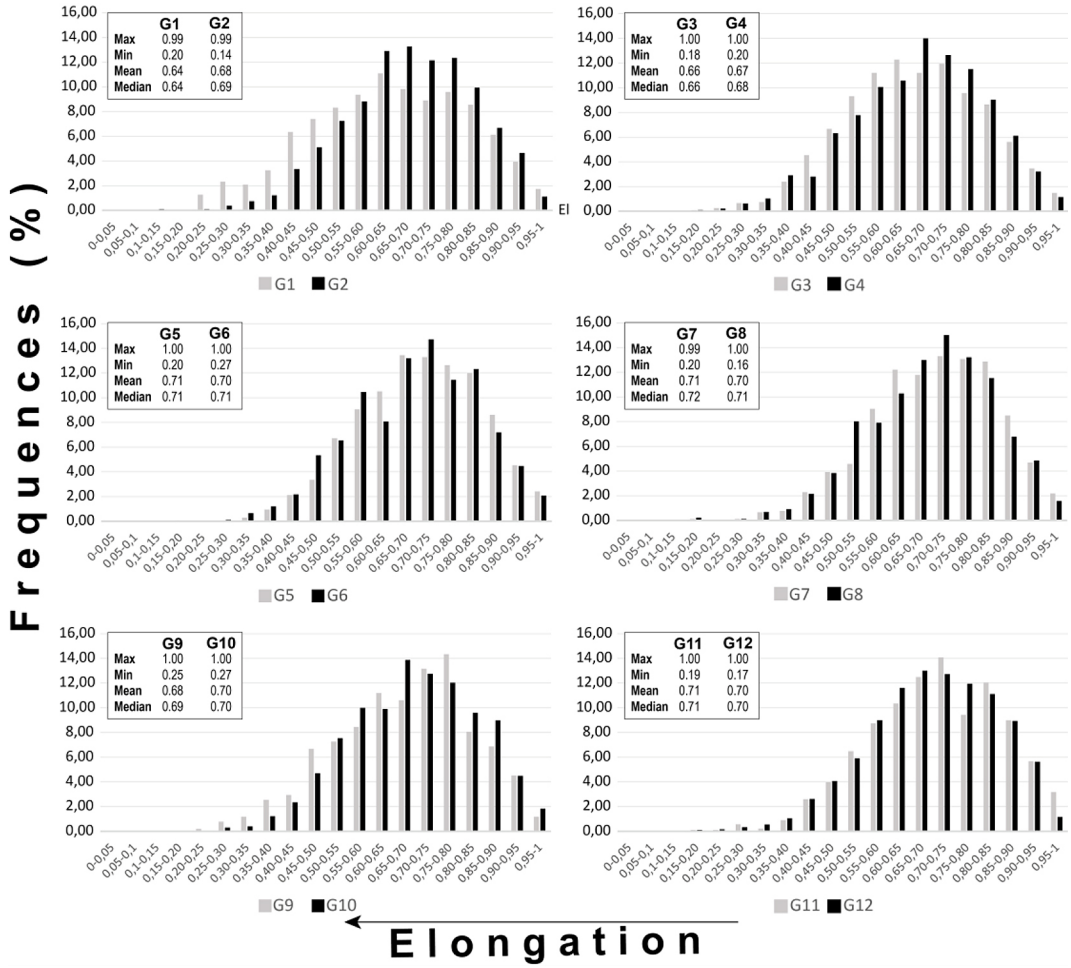


**Figure 12.** Evolution of the Ei frequencies of pebbles within the studied stations

that those stations lack or nearly lack extremely and very elongated pebbles (Ei: 0–0.4). Regarding the distribution modes of Ei:

- Stations G1, G6, G8, and G11 exhibit a trimodal pattern;
- G3, G7, G9, and G10 display a bimodal distribution;
- G4, G5, and G12 demonstrate a distribution pattern with a single mode.

In contrast to the preceding graph, the subsequent figure illustrates the frequency distribution of each broad class of pebble elongation across the successive studied stations. This distinct statistical representation reinforces the earlier findings. Notably, slightly elongated pebbles are highly prevalent, accounting for approximately 40% to 52% of the total, with a peak frequency of around 52% observed at G8 and a minimum proportion of 39% at G1.

Not elongated and moderately elongated pebbles occur in nearly equal proportions, ranging from approximately 20% to 30%. However, moderately elongated pebbles occasionally exceed 30% (e.g., G1 and G3), while the pebbles of the other class do not surpass this value. The second discrepancy emerges in the upstream-downstream evolution of frequencies within these two classes. Moderately elongated pebbles tend to decrease in the downstream direction, whereas not elongated ones exhibit a tendency to be more abundant in the last stations compared to the first ones. Very elongated pebbles do not exceed 10% of the studied clasts in any station, with the highest value of this class observed at G10, followed by G4 and G9. Extremely elongated pebbles have negligible frequencies within the middle Inaouène reach (Figure 13).

Considering the mean and median values of Ei, their evolution demonstrates slight variations from station to station, but overall, there is a downstream increase from 0.64 at G1 to approximately 0.70 at G12, indicating a slight decrease in elongation (Figure 14). In detail, three cycles of increase-decrease of Ei means/medians are depicted by the following curves (i.e., a decrease-increase of elongation). The first peaks at G2, the second at G7, and the third at G11. These peaks represent stations where Ei/elongation is high/low, while the troughs indicate stations where Ei/elongation is low/high. It's noteworthy that the highest mean and median values of Ei occur at G7 (i.e., lowest elongation), while the lowest mean/median of Ei occur at G1 (i.e., highest elongation).

Regarding the spatial occurrence of these cycles, the second cycle exhibits the longest path of occurrence, spanning seven stations from G3 to G9. The last cycle ranks second, covering four stations from G9 to G12, while the first one shows the shortest cycle with only three stations (from G1 to G3).

Across various stations, the analysis of Ci frequencies reveals a spectrum of results (Figure 15). Generally, the highest detected Ci value among all stations is approximately 0.99, indicating some pebbles with maximal circularity, whereas the lowest ranges from 0.34 (indicating moderate circularity) at G2 to 0.5 (also indicating moderate circularity) at G6. Mean values fluctuate from 0.76 at G1 to 0.82 at G5, G7, and G11, all classified as highly circular pebbles. The collective average of

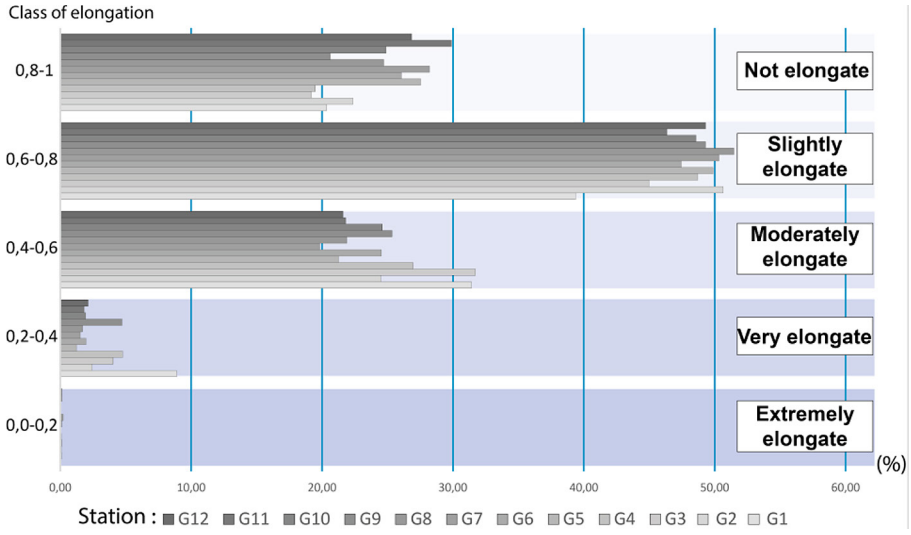


**Figure 13.** Frequencies and classes of elongation of the studied pebbles across the Middle Inaouène reach

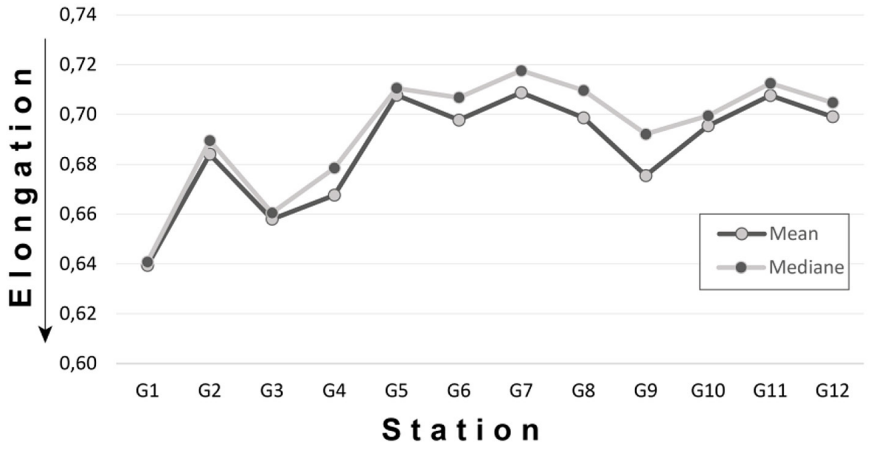


**Figure 14.** Downstream variability of pebbles' elongation within the Middle Inaouène

these mean values approximates 0.80, indicating that the typical pebbles within the Inaouène River exhibit high circularity. The tallest bars, representing the maximum values of class frequencies, depict that predominantly, all stations harbor pebbles with high and sometimes very high circularity (Ci: ~ 0.75–0.90). Conversely, minimal or zero values of these frequencies suggest that certain stations lack or nearly lack pebbles with low to very low circularity (Ci: 0–0.55).

When it comes to the distribution modes of Ci, only station G1 exhibits a bimodal pattern,

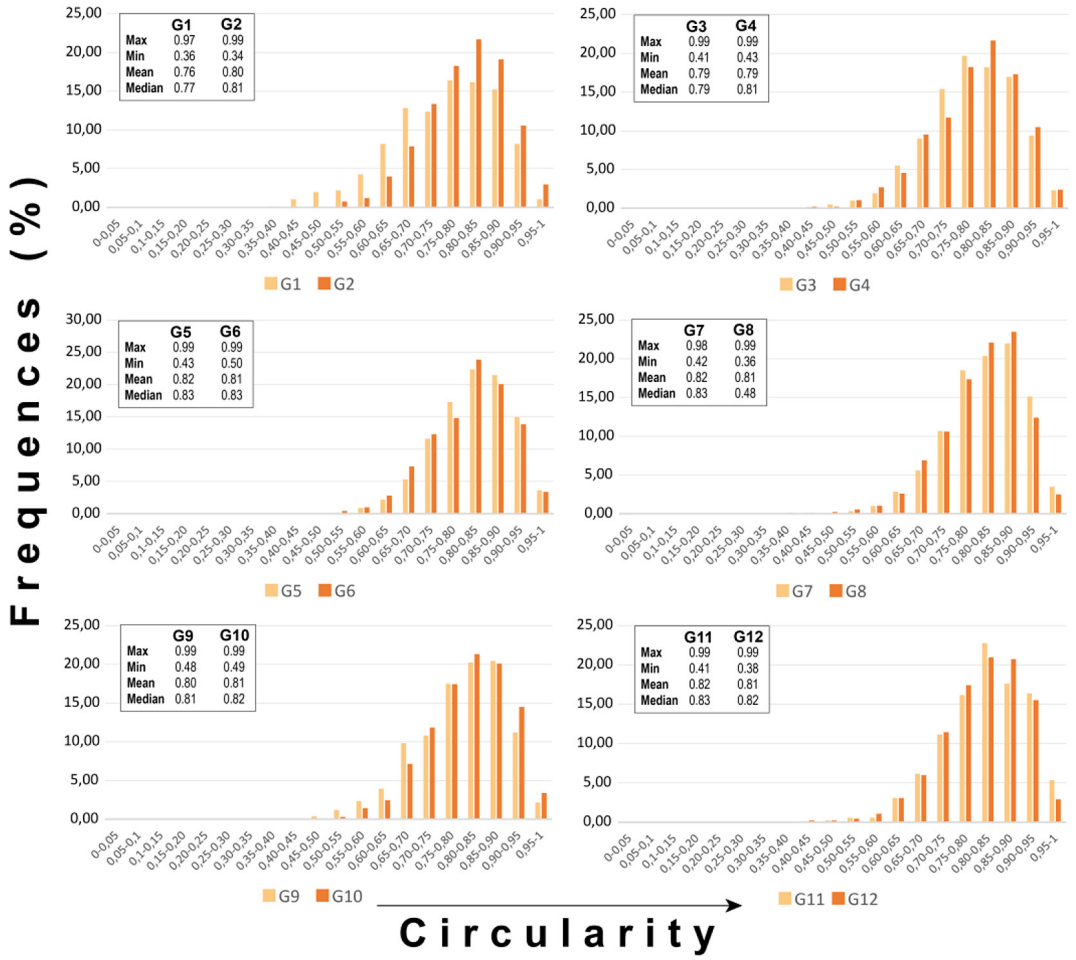


**Figure 15.** Evolution of the Ci frequencies of pebbles within the studied stations

while all the other successive stations display a single-mode distribution.

Unlike the previous graph, the following figure portrays the frequency distribution of each major category of pebble circularity across the consecutive stations under study. This unique statistical depiction strengthens the previous conclusions. Noteworthy is the dominance of highly circular pebbles, comprising roughly 40% to 52% of the total, with the highest frequency peaking at around 52% noted at G8 and the lowest proportion of about 39% observed at G1.

The second most abundant circularity class in this set of pebbles is the moderate circularity category, comprising approximately 26% of pebbles at G12 to about 37% at G1 and G3. While there is a pattern of fluctuation of these pebbles along the studied channel (e.g., from G4 to G10), there is a general trend of the associated frequencies from G1 to G12. The next most representative circularity class of the studied pebbles is the very high circularity category. Pebbles associated with this class constitute approximately 11% at G1 to 24% at G11. Fluctuations in frequencies also occur within this class; however, the general evolutionary pattern this time shows an increase in the number of very highly circular pebbles downstream. The less abundant pebbles in terms of circularity are the low circular pebbles, with frequencies within this class ranging from around 3% at G5 and G7 to about 13% at G1. Very low circular pebbles exhibit very low or even negligible frequencies, indicating a significant absence of this category within the studied reach of the Inaouène (Figure 16).

Across stations, both the mean and median values of Ci show slight variations, with an overall downstream trend from ~ 0.76 at G1 to approximately 0.81 at G12, suggesting a mild increase in circularity. Notably, this evolution is marked by three cycles of increase and decrease in Ci means/medians represented by distinct curves. The peaks of these curves occur at G2, G7, and G11, indicating stations with high circularity (Ci) values. Conversely, the troughs denote stations with opposite Ci characteristics. Interestingly, G7 exhibits the highest mean and median Ci values, indicating the highest circularity, while G1 displays the lowest mean/median Ci values, indicating the lowermost circularity (Figure 17).

In terms of their spatial distribution, the second cycle stands out for its extensive occurrence, stretching across seven stations from G3 to G9. Following this, the last cycle encompasses four stations from G9 to G12, while the initial cycle presents the shortest span, involving only three stations from G1 to G3.

## DISCUSSION

Before developing any interpretations, it is worth recalling the initial aim of this study. This work primarily focuses on applying semi-automatic method to establish the downstream variability of pebbles' grain size and shape along the middle reach of the Inaouène. In light of the resulting data, this section attempts to discuss this variation and provide a general perspective on the potential future implications of these findings.

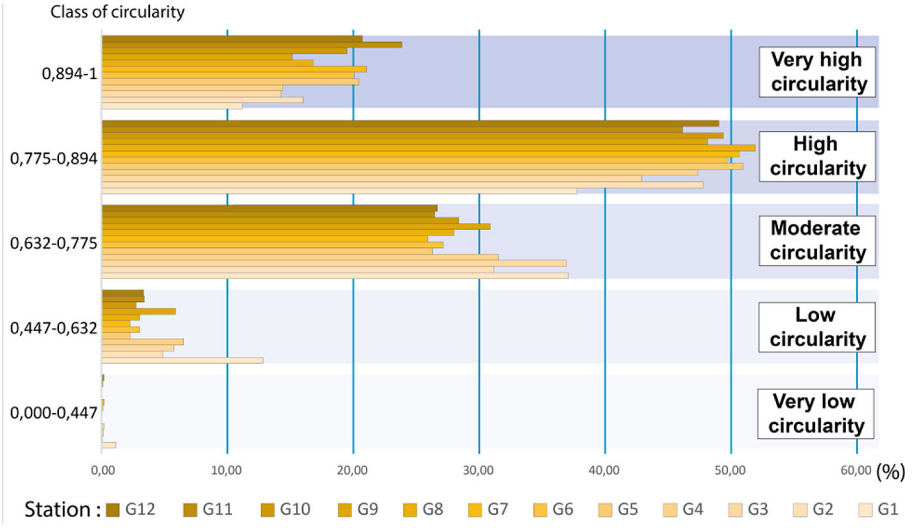


**Figure 16.** Frequencies and classes of circularity of the studied pebbles across the Middle Inaouènereach

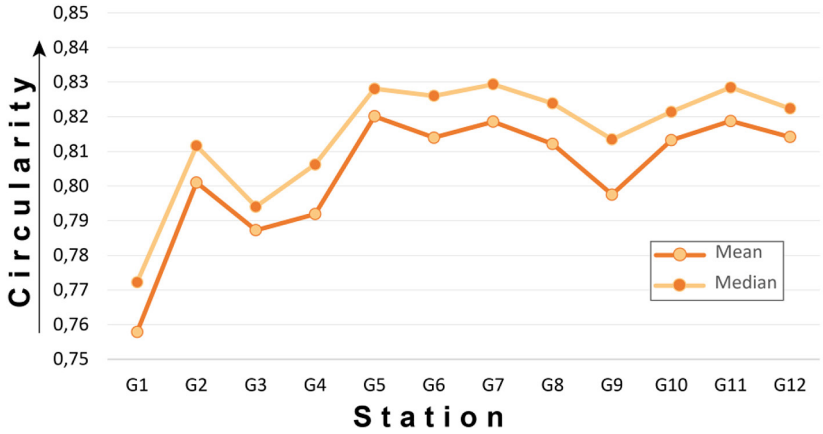


**Figure 17.** Downstream variability of pebbles' circularity within the Middle Inaouène

The image-based software BASEGRAIN enables quantitative monitoring of the size, sorting, and shape of pebbles along the middle Inaouène River. This method is fast and resource-efficient, providing precise data that can be used to assess the geomorphic evolution of the channel and to provide accurate information about river conditions. These insights have significant implications for decision-making and river management.

Broadly, the downstream variability of pebbles is influenced by travel distance, transport capacity, and sediment inputs from tributaries. The travel distance is proportional to downstream grain-size fining and sorting, as well as changes in shape, with circularity increasing and elongation decreasing (Brewer and Lewin, 1993; McPherson, 1971; Roussillon et al., 2009; Wentworth, 1922). Transport capacity affects pebbles similarly, influenced by water discharge and slope (Parker, 2013; Xiao et al., 2017). Conversely, lateral sediment input is inversely proportional to these downstream changes in pebbles (Parker, 2013). The first proportional relationships are carried trough abrasion and particles fragmentation (Pokhrel et al., 2024), while the inversely correlated one is controlled by the lithology of the source rock and the degree of weathering prior to introduction into the fluvial environment (Javanbakht et al., 2022; Pokhrel et al., 2024).

The grain-size parameters (i.e., d50, d90, b-max) generally decrease along the Inaouène channel, with the exception of d30, which remains relatively constant due to the software's limited capacity to accurately quantify the fine fraction. Additionally, circularity and grain sorting increase while elongation decreases, following the typical trend expected given the long distance between the first and last stations (~60 km) and the abrasive effects on pebbles. However, the internal variations in these parameters are controlled by transport capacity and lateral inputs.

We attribute the relatively rapid decrease in grain-size parameters and elongation, along with the increase in circularity from G1 to G6, to the high gradient of the river profile in the headwaters of the valley, where the average slope reaches 2.8%. As the gradient decreases to 1% in the downland, changes in these characteristics either slow down or fluctuate around similar values.

Peaks in grain size observed at G4, G8, and G11 can be attributed to lateral inputs from nearby tributaries, introducing basalt at G4 and sandstone elements at G8 and G11. The sorting index also reflects this trend, with peaks at G4, G8, and G9 explained similarly, as the introduction of new elements decreases sorting.

The peaks in SI and circularity (i.e., troughs in elongation) at G2 and G5 cannot be explained by the aforementioned reasons. Instead, these patterns likely reflect the recycling of multigenerational pebbles (Quick et al., 2019). Station G9 shows poorly sorted pebbles with a peak in elongation and a trough in circularity, indicating a similar effect of multicyclic transport. The former reason can explain also the multimodal distribution of pebbles' shape within several stations.

The results obtained from this downstream monitoring can be utilized in various ways. Three essential applications of this data include: geomorphological applications, Ecological practices, river management and restoration.

On the geomorphological level, this data, particularly the d50 value, can be used to classify

the stream type according to established stream classification systems like the Rosgen classification (Rosgen, 1994). By conducting the same measurements over time at the same locations, changes in streambed sediments can be tracked, supporting sediment supply calculations. This allows for monitoring the impacts of land use changes or other factors affecting sediment supply and transport in the stream (Olsen et al., 2005). These changes can also be used to predict the evolution of channel morphology at each site, as sediment size and shape influence the equilibrium channel form (Wolman and Brush, 1961). Furthermore, the downstream evolution of pebble shape provides insights into the provenance and transport history of river sediments (Litty and Schlunegger, 2017; Pokhrel et al., 2024). These data can also be used in paleohydrological reconstructions. Similar measurements have been applied to calculate the settling velocity of pebbles within the channel during the Late Pleistocene (Kumar et al., 2020).

To our knowledge, no ecological survey has been conducted in the Inaouène channel that involves the physical and geomorphic aspects of the channel. For these ecological practices, pebbles' size and shape are key determinants of the physical habitat structure in rivers, influencing factors like substrate stability, interstitial space, and flow patterns. For example, sites with fine pebbles and a low fraction of fine sandy-silty material provide good habitats for spawning of the Atlantic salmonid in mountainous alluvial rivers (Hauer et al., 2015). Monitoring spatiotemporal changes in pebble characteristics can help assess the suitability of river habitats for different aquatic organisms, such as spawning grounds for fish or refugia for macroinvertebrates. Furthermore, pebble abrasion contributes to the production of fine sediments, which can have both positive and negative impacts on aquatic ecosystems. Fine sediments can degrade water quality, smother benthic habitats, and disrupt the feeding and spawning of aquatic organisms. However, they can also provide nutrients and substrate for some species. Understanding the rates and patterns of pebble abrasion can help predict the timing and magnitude of fine sediment pulses, allowing for better management of their ecological impacts (Bilotta and Brazier, 2008; Kemp et al., 2011).

Regarding river restoration and management, understanding pebbles' size and shape evolution can inform the design of stable, self-sustaining channels and the selection of suitable bed material for restoration projects. Predicting the long-term changes in pebble characteristics aids in assessing the sustainability and resilience of river engineering solutions. Additionally, monitoring pebble abrasion rates can forecast fine sediment production, guiding decisions on sediment management, such as the placement of sediment traps or the timing of dredging operations (Kondolf, 1995; Owens et al., 2005; Wilcock and Crowe, 2003; Wohl et al., 2015).

## CONCLUSIONS

In this study, semi-automatic methods were employed for the first time to monitor the downstream variability of pebbles' size and shape within the middle Inaouène Valley, using 12 sampling stations. These methods involved image-based analysis and BASEGRAIN software, complemented by manual sampling to support the numerical process.

Overall, the middle Inaouène channel typically contains highly circular, slightly elongated, pebble-sized gravels, with d50 values ranging between 25 and 60 mm. Downstream, the system exhibits general fining and sorting, with an increase in circularity and a decrease in elongation, attributed to the abrasion and fragmentation of gravels transported within the channel. From station to station, the pebbles show clear variability in size and shape, with rapid changes in the first six stations and slower or negligible changes in the downstream stations, following the general decrease in the river profile gradient. Internal peaks or troughs are linked to either lateral supply from tributaries or the effect of recycling transport, which mixes different populations of gravels at the same site.

The results of this survey have significant implications for future projects in geomorphological studies, ecological assessments, and river restoration or engineering interventions. The semi-automatic methods used in this study proved efficient in terms of time and resource consumption, providing accurate measurements of coarse gravels similar to those obtained through manual assessments. However, these techniques have limitations, becoming increasingly inaccurate as pebble size decreases and when particles are not lying flat or fully visible during photographing.

## REFERENCES


1. Al-Rousan, T., Masad, E., Tutumluer, E., Pan, T., 2007. Evaluation of image analysis techniques for quantifying aggregate shape characteristics. Construction and Building Materials 21, 978–990. https://doi.org/10.1016/j.conbuildmat.2006.03.005
2. Baynes, E.R.C., Lague, D., Steer, P., Bonnet, S., Illien, L., 2020. Sediment flux-driven channel geometry adjustment of bedrock and mixed gravel–bedrock rivers. Earth Surface Processes and Landforms 45, 3714–3731. https://doi.org/10.1002/esp.4996
3. Benzougagh, B., Meshram, S.G., Baamar, B., Dridri, A., Boudad, L., Sadkaoui, D., Mimich, K., 2020. Relationship between landslide and morphostructural analysis: a case study in Northeast of Morocco. Applied Water Science 10, 175. https://doi.org/10.1007/s13201-020-01258-4
4. Benzougagh, B., Meshram, S.G., Dridri, A., Boudad, L., Baamar, B., Sadkaoui, D., Khedher, K.M., 2021. Identification of critical watershed at risk of soil erosion using morphometric and geographic information system analysis. Applied Water Science 12, 8. https://doi.org/10.1007/s13201-021-01532-z
5. Bilotta, G.S., Brazier, R.E., 2008. Understanding the influence of suspended solids on water quality and aquatic biota. Water Research 42, 2849–2861. https://doi.org/10.1016/j.watres.2008.03.018
6. Blott, S.J., Pye, K., 2008. Particle shape: a review and new methods of characterization and classification. Sedimentology 55, 31–63. https://doi.org/10.1111/j.1365-3091.2007.00892.x
7. Brahim, B., Dridri, A., Boudad, L., Ossama, K., Drisss, S., Hmad, B., 2017. Evaluation of natural hazard of Inaouene Watershed River in Northeast of Morocco: Application of Morphometric and Geographic Information System approaches 85–97.
8. Brahim, B., Meshram, S.G., Abdallah, D., Larbi, B., Drisss, S., Khalid, M., Khedher, K.M., 2020. Mapping of soil sensitivity to water erosion by RUSLE model: case of the Inaouene watershed (Northeast Morocco). Arabian Journal of Geosciences 13, 1153. https://doi.org/10.1007/s12517-020-06079-y
9. Brewer, P.A., Lewin, J., 1993. In-transport modification of alluvial sediment: Field evidence and laboratory experiments, in: Alluvial Sedimentation. John Wiley & Sons, Ltd, 23–35. https://doi.org/10.1002/9781444303995.ch3
10. Bunte, K., Abt, S.R., 2001. Sampling surface and subsurface particle-size distributions in wadable gravel-and cobble-bed streams for analyses in sediment transport, hydraulics, and streambed monitoring. Gen. Tech. Rep. RMRS-GTR-74. Fort Collins,CO: U.S. Department of Agriculture, Forest Service, Rocky Mountain Research Station. 428, 74. https://doi.org/10.2737/RMRS-GTR-74
11. Charpentier, I., Sarocchi, D., Rodriguez Sedano, L.A., 2013. Particle shape analysis of volcanic clast samples with the Matlab tool MORPHEO. Computers & Geosciences 51, 172–181. https://doi.org/10.1016/j.cageo.2012.07.015
12. Church, M., Jones, D., 1982. Channel bars in gravel-bed rivers. Gravel-bed rivers 1092, 291–1093.
13. Condit, C.D., Chavez, P.S., 1979. Basic concepts of computerized digital image processing for geologists (No. 1462), Bulletin. U.S. Govt. Print. Off.,. https://doi.org/10.3133/b1462
14. Crosa, G., Castelli, E., Gentili, G., Espa, P., 2010. Effects of suspended sediments from reservoir flushing on fish and macroinvertebrates in an alpine stream. Aquat. Sci. 72, 85–95. https://doi.org/10.1007/s00027-009-0117-z
15. Daniels, M.D., McCusker, M.H., 2010. Operator bias characterizing stream substrates using Wolman pebble counts with a standard measurement template. Geomorphology 115, 194–198. https://doi.org/10.1016/j.geomorph.2009.09.038
16. D'Arcy, M., Whittaker, A.C., Roda-Boluda, D.C., 2017. Measuring alluvial fan sensitivity to past climate changes using a self-similarity approach to grain-size fining, Death Valley, California. Sedimentology 64, 388–424. https://doi.org/10.1111/sed.12308
17. Detert, M., Kadinski, L., Weitbrecht, V., 2018. On the way to airborne gravelometry based on 3D spatial data derived from images. International Journal of Sediment Research 33, 84–92. https://doi.org/10.1016/j.ijsrc.2018.02.001
18. Detert, M., Weitbrecht, V., 2013. User guide to gravelometric image analysis by BASEGRAIN.
19. Detert, M., Weitbrecht, V., 2012. Automatic object detection to analyze the geometry of gravel grains - A free stand-alone tool. River Flow 2012 - Proceedings of the International Conference on Fluvial Hydraulics 1, 595–600.
20. Eaton, B.C., Moore, R.D., MacKenzie, L.G., 2019. Estimating confidence intervals for gravel bed surface grainsize distributions (preprint). Physical: Geomorphology (including all aspects of fluvial, coastal, aeolian, hillslope and glacial geomorphology). https://doi.org/10.5194/esurf-2019-4
21. Fehr, R., 1987. Einfache Bestimmung der Korngrössenverteilung von Geschiebematerial mit Hilfe der Linienzahlanalyse [Simple detection of grain size distribution of sediment material using line-by-number analysis]. Schweizer Ingenieur und Architekt 105, 1104–1109. https://doi.org/10.5169/seals-76710
22. Folk, R.L., 1974. Petrology of sedimentary rocks: Austin. Texas, Hemphill, 182.
23. Galia, T., 2017. Geomorphology and Hydraulics of Steep Mountain Channels, in: Open Channel Hydraulics, River Hydraulic Structures and Fluvial

Geomorphology. CRC Press.

24. Garouani, A.E., Tribak, A., 2006. Relation entre hydrologie et climat dans le bassin versant de l'Oued Inaouène (pré-Rif marocain) 7.
25. Geist, J., Auerswald, K., 2007. Physicochemical stream bed characteristics and recruitment of the freshwater pearl mussel (*Margaritifera margaritifera*). Freshwater Biology 52, 2299–2316. https://doi.org/10.1111/j.1365-2427.2007.01812.x
26. Graham, D.J., Reid, I., Rice, S.P., 2005a. Automated sizing of coarse-grained sediments: image-processing procedures. Math Geol 37, 1–28. https://doi.org/10.1007/s11004-005-8745-x
27. Graham, D.J., Rice, S.P., Reid, I., 2005b. A transferable method for the automated grain sizing of river gravels. Water Resources Research 41. https://doi.org/10.1029/2004WR003868
28. Green, J.C., 2003. The precision of sampling grain-size percentiles using the Wolman method. Earth Surface Processes and Landforms 28, 979–991. https://doi.org/10.1002/esp.513
29. Guerit, L., Barrier, L., Liu, Y., Narteau, C., Lajeunesse, E., Gayer, E., Métivier, F., 2018. Uniform grain-size distribution in the active layer of a shallow, gravel-bedded, braided river (the Urumqi River, China) and implications for paleo-hydrology. Earth Surface Dynamics 6, 1011–1021. https://doi.org/10.5194/esurf-6-1011-2018
30. Guerit, L., Barrier, L., Narteau, C., Métivier, F., Liu, Y., Lajeunesse, E., Gayer, E., Meunier, P., Malverti, L., Ye, B., 2014. The grain-size patchiness of braided gravel-bed streams & ndash; example of the Urumqi River (northeast Tian Shan, China). Advances in Geosciences 37, 27–39. https://doi.org/10.5194/adgeo-37-27-2014
31. Hauer, C., 2015. Review of hydro-morphological management criteria on a river basin scale for preservation and restoration of freshwater pearl mussel habitats. Limnologica, The current status and future challenges for the preservation and conservation of freshwater pearl mussel habitats 50, 40–53. https://doi.org/10.1016/j.limno.2014.11.002
32. Hauer, C., Pulg, U., Gabrielsen, S.-E., Barlaup, B.T., 2015. Application of step-backwater modelling for salmonid spawning habitat restoration in Western Norway. Ecohydrology 8, 1239–1261. https://doi.org/10.1002/eco.1578
33. Hauer, C., Unfer, G., Habersack, Pulg, U., Schnell, 2013. Bedeutung von Flussmorphologie und Sedimenttransport in Bezug auf die Qualitat und Nachhaltigkeit von Kieslaichplatzen. KW-Korrespondenz Wasserwirtschaft 6, 189–197. https://doi.org/10.3243/kwe2013.04.002
34. Ibbeken, H., Schleyer, R., 1986. Photo-sieving: A method for grain-size analysis of coarse-grained, unconsolidated bedding surfaces. Earth Surface Processes and Landforms 11, 59–77. https://doi.org/10.1002/esp.3290110108
35. Ingram, R.L., 1971. Sieve analysis. Procedures in sedimentary petrology 49–67.
36. Javanbakht, M., Beheshtipur, M.R., Raftari Farimani, S., 2022. Factors affecting average grain size changes in rivers of a catchment area (Ardak catchment area, northeast Iran). Arab J Geosci 15, 448. https://doi.org/10.1007/s12517-021-08512-2
37. Jerolmack, D.J., 2013. Pebbles on Mars. Science 340, 1055–1056. https://doi.org/10.1126/science.1239343
38. Kellerhals, R., Bray, D.I., 1971. Sampling procedures for coarse fluvial sediments. Journal of the Hydraulics Division 97, 1165–1180. https://doi.org/10.1061/JYCEAJ.0003044
39. Kemp, P., Sear, D., Collins, A., Naden, P., Jones, I., 2011. The impacts of fine sediment on riverine fish. Hydrological Processes 25, 1800–1821. https://doi.org/10.1002/hyp.7940
40. Kondolf, G.M., 1995. Geomorphological stream channel classification in aquatic habitat restoration: Uses and limitations. Aquatic Conservation: Marine and Freshwater Ecosystems 5, 127–141. https://doi.org/10.1002/aqc.3270050205
41. Kondolf, G.M., Wolman, M.G., 1993. The sizes of salmonid spawning gravels. Water Resources Research 29, 2275–2285. https://doi.org/10.1029/93WR00402
42. Köster, E., Leser, H., 1967. Geomorphologie: Bodenkundliche Methoden. Morphometrie und Granulometrie. Westermann.
43. Kozakiewicz, J., 2013. Automated Image Analysis for Measuring Size and Shape of Martian Sand Grains: A Tool to Estimate Threshold Shear Velocities and to Compare Different Sand Samples, in: 44th Annual Lunar and Planetary Science Conference. 2906.
44. Krumbein, W.C., 1941. Measurement and geological significance of shape and roundness of sedimentary particles. Journal of Sedimentary Research 11, 64–72. https://doi.org/10.1306/D42690F3-2B26-11D7-8648000102C1865D
45. Kumar, A., Srivastava, P., Devrani, R., 2020. Using clast geometries to establish paleoriver discharges: Testing records for aggradation and incision from the upper Indus River, Ladakh Himalaya. Geomorphology 362, 107202. https://doi.org/10.1016/j.geomorph.2020.107202
46. Laaraj, M., Benaabidate, L., Mesnage, V., 2020. Assessment of Inaouene River Pollution for potable water supply, Northern Morocco. Journal of Ecological Engineering 21. https://doi.org/10.12911/22998993/125450
47. Laaraj, M., Mesnage, V., Nabih, S., Mliyeh, M.M., Lahmidi, I., Benaabidate, L., 2022. Assessment of heavy metals in the sediments of the inaouene

watershed upstream the idriss 1 st dam, Northern Morocco. J. Ecol. Eng. 23, 157–170. https://doi.org/10.12911/22998993/151843

48. Lahsaini, M., Tabyaoui, H., Mounadel, A., Bouderka, N., Lakhili, F., 2018. Comparison of SRTM and ASTER derived digital elevation models of Inaouene River Watershed (North, Morocco)—Arc Hydro Modeling. Journal of Geoscience and Environment Protection 06, 141. https://doi.org/10.4236/gep.2018.69011
49. Libiad, M., Abdelmajid, K., Abdeslam, E., 2012. Végétation ripicole et gestion des eaux de surface, cas du 29.
50. Litty, C., Schlunegger, F., 2017. Controls on pebbles' size and shape in streams of the Swiss Alps. The Journal of Geology 125, 101–112. https://doi.org/10.1086/689183
51. Maerz, N.H., Palangio, T.C., Franklin, J.A., 1996. WipFrag image based granulometry system, in: Measurement of Blast Fragmentation. Routledge.
52. Marouane, L., Lahcen, B., Valérie, M., 2021. Assessment and mapping of water erosion by the integration of the Gavrilovic "EPM" model in the Inaouene watershed, Morocco. E3S Web Conf. 314, 03009. https://doi.org/10.1051/e3sconf/202131403009
53. McPherson, H.J., 1971. Downstream changes in sediment character in a high energy mountain stream channel. Arctic and Alpine Research 3, 65–79. https://doi.org/10.2307/1550383
54. Michard, A., Saddiqi, O., Chalouan, A., Frizon de Lamotte, D. (Eds.), 2010. Continental evolution: the geology of Morocco; structure, stratigraphy, and tectonics of the Africa-Atlantic-Mediterranean Triple Junction, Lecture notes in earth sciences. Springer, Berlin Heidelberg.
55. Morel, J.-L., 1992. Carte des mouvements récents du Rif. N°365.
56. Müller, G., 1967. Methods in sedimentary petrology.
57. Naoura, J., Benaabidate, L., Dridri, A., 2012. Hydrology and surface water quality of the inaouene river watershed, Morocco. Presented at the Sixteenth International Water Technology Conference, Istanbul, Turkey, 12.
58. Olsen, D.S., Roper, B.B., Kershner, J.L., Henderson, R., Archer, E., 2005. Sources of variability in conducting pebble counts: their potential influence on the results of stream monitoring programs1. JAWRA Journal of the American Water Resources Association 41, 1225–1236. https://doi.org/10.1111/j.1752-1688.2005.tb03796.x
59. Owens, P.N., Batalla, R.J., Collins, A.J., Gomez, B., Hicks, D.M., Horowitz, A.J., Kondolf, G.M., Marden, M., Page, M.J., Peacock, D.H., Petticrew, E.L., Salomons, W., Trustrum, N.A., 2005. Fine-grained sediment in river systems: environmental significance and management issues. River Research and Applications 21, 693–717. https://doi.org/10.1002/rra.878
60. Parker, G., 2013. Transport of Gravel and Sediment Mixtures 165–251. https://doi.org/10.1061/9780784408148.ch03
61. Parker, G., Klingeman, P.C., McLean, D.G., 1982. Bedload and size distribution in paved gravel-bed streams. Journal of the Hydraulics Division 108, 544–571. https://doi.org/10.1061/JYCEAJ.0005854
62. Pokhrel, P., Attal, M., Sinclair, H.D., Mudd, S.M., Naylor, M., 2024. Downstream rounding rate of pebbles in the Himalaya. Earth Surface Dynamics 12, 515–536. https://doi.org/10.5194/esurf-12-515-2024
63. Powers, M.C., 1953. A new roundness scale for sedimentary particles. Journal of Sedimentary Research 23, 117–119. https://doi.org/10.1306/D4269567-2B26-11D7-8648000102C1865D
64. Pulg, U., Barlaup, B.T., Sternecker, K., Trepl, L., Unfer, G., 2013. Restoration of spawning habitats of brown trout (*salmo Trutta*) in a Regulated chalk stream. River Research and Applications 29, 172–182. https://doi.org/10.1002/rra.1594
65. Purinton, B., Bookhagen, B., 2021. Tracking downstream variability in large grain-size distributions in the south-central Andes. Journal of Geophysical Research: Earth Surface 126, e2021JF006260. https://doi.org/10.1029/2021JF006260
66. Quick, L., Sinclair, H.D., Attal, M., Singh, V., 2019. Conglomerate recycling in the Himalayan foreland basin: Implications for grain size and provenance. GSA Bulletin 132, 1639–1656. https://doi.org/10.1130/B35334.1
67. Rice, S., Church, M., 1996. Sampling surficial fluvial gravels; the precision of size distribution percentile sediments. Journal of Sedimentary Research 66, 654–665. https://doi.org/10.2110/jsr.66.654
68. Rosgen, D.L., 1994. A classification of natural rivers. CATENA 22, 169–199. https://doi.org/10.1016/0341-8162(94)90001-9
69. Roussillon, T., Piégay, H., Sivignon, I., Tougne, L., Lavigne, F., 2009. Automatic computation of pebble roundness using digital imagery and discrete geometry. Computers & Geosciences 35, 1992–2000. https://doi.org/10.1016/j.cageo.2009.01.013
70. Sibari, H., Haida, S., Foutlane, M., 2018. Estimation of particle material and dissolved flows during floods in the Inaouene Watershed. (Northeast Of Morocco). E3S Web Conf. 37, 04004. https://doi.org/10.1051/e3sconf/20183704004
71. Snoussi, M., Haïda, S., Imassi, S., 2002. Effects of the construction of dams on the water and sediment fluxes of the Moulouya and the Sebou Rivers, Morocco. Reg Environ Change 3, 5–12. https://doi.org/10.1007/s10113-001-0035-7

72. Sochan, A., Zieliński, P., Bieganowski, A., 2015. Selection of shape parameters that differentiate sand grains, based on the automatic analysis of two-dimensional images. Sedimentary Geology 327, 14–20. https://doi.org/10.1016/j.sedgeo.2015.07.007
73. Soloy, A., Turki, I., Fournier, M., Costa, S., Peuziat, B., Lecoq, N., 2020. A deep learning-based method for quantifying and mapping the grain size on pebble beaches. Remote Sensing 12, 3659. https://doi.org/10.3390/rs12213659
74. Stähly, S., Friedrich, H., Detert, M., 2017. Size ratio of fluvial grains' intermediate axes assessed by image processing and square-hole sieving. Journal of Hydraulic Engineering 143, 06017005. https://doi.org/10.1061/(ASCE)HY.1943-7900.0001286
75. Steer, P., Guerit, L., Lague, D., Crave, A., Gourdon, A., 2022. Size, shape and orientation matter: fast and semi-automatic measurement of grain geometries from 3D point clouds. Earth Surface Dynamics 10, 1211–1232. https://doi.org/10.5194/esurf-10-1211-2022
76. Strom, K.B., Kuhns, R.D., Lucas, H.J., 2010. Comparison of automated image-based grain sizing to standard pebble-count methods. Journal of Hydraulic Engineering 136, 461–473. https://doi.org/10.1061/(ASCE)HY.1943-7900.0000198
77. Sun, W., Wang, L., Tutumluer, E., 2012. Image analysis technique for aggregate morphology analysis with two-dimensional fourier transform method. Transportation Research Record 2267, 3–13. https://doi.org/10.3141/2267-01
78. Suter, G., 1980. Carte géologique de la chaîne rifaine, v. N°245a.
79. Sutherland, A.B., Meyer, J.L., Gardiner, E.P., 2002. Effects of land cover on sediment regime and fish assemblage structure in four southern Appalachian streams. Freshwater Biology 47, 1791–1805. https://doi.org/10.1046/j.1365-2427.2002.00927.x
80. Szabó, T., Domokos, G., Grotzinger, J.P., Jerolmack, D.J., 2015. Reconstructing the transport history of pebbles on Mars. Nat Commun 6, 8366. https://doi.org/10.1038/ncomms9366
81. Tafesse, S., 2012. Physical characterization of coarse clasts with 3D image-analysis method : development, evaluation and application.
82. Tafesse, S., Fernlund, J.M.R., Bergholm, F., 2012. Digital sieving-Matlab based 3-D image analysis. Engineering Geology 137–138, 74–84. https://doi.org/10.1016/j.enggeo.2012.04.001
83. Tunwal, M., Mulchrone, K.F., Meere, P.A., 2020. Image based particle shape analysis toolbox (IPSAT). Computers & Geosciences 135, 104391. https://doi.org/10.1016/j.cageo.2019.104391
84. Vangla, P., Roy, N., Gali, M.L., 2017. Image based shape characterization of granular materials and its effect on kinematics of particle motion. Granular Matter 20, 6. https://doi.org/10.1007/s10035-017-0776-8
85. Wadell, H., 1935. Volume, shape, and roundness of quartz particles. The Journal of Geology 43, 250–280. https://doi.org/10.1086/624298
86. Wadell, H., 1933. Sphericity and roundness of rock particles. The Journal of Geology 41, 310–331. https://doi.org/10.1086/624040
87. Watkins, S.E., Whittaker, A.C., Bell, R.E., Brooke, S.A.S., Ganti, V., Gawthorpe, R.L., McNeill, L.C., Nixon, C.W., 2020. Straight from the source's mouth: Controls on field-constrained sediment export across the entire active Corinth Rift, central Greece. Basin Research 32, 1600–1625. https://doi.org/10.1111/bre.12444
88. Wentworth, C.K., 1922. A scale of grade and class terms for clastic sediments. The Journal of Geology 30, 377–392. https://doi.org/10.1086/622910
89. Wilcock, P.R., Crowe, J.C., 2003. Surface-based transport model for mixed-size sediment. Journal of Hydraulic Engineering 129, 120–128. https://doi.org/10.1061/(ASCE)0733-9429(2003)129:2(120)
90. Wohl, E., Bledsoe, B.P., Jacobson, R.B., Poff, N.L., Rathburn, S.L., Walters, D.M., Wilcox, A.C., 2015. The natural sediment regime in rivers: Broadening the foundation for ecosystem management. BioScience 65, 358–371. https://doi.org/10.1093/biosci/biv002
91. Wohl, E.E., Anthony, D.J., Madsen, S.W., Thompson, D.M., 1996. A comparison of surface sampling methods for coarse fluvial sediments. Water Resources Research 32, 3219–3226. https://doi.org/10.1029/96WR01527
92. Wolcott, J., Church, M., 1991. Strategies for sampling spatially heterogeneous phenomena; the example of river gravels. Journal of Sedimentary Research 61, 534–543. https://doi.org/10.1306/D4267753-2B26-11D7-8648000102C1865D
93. Wolman, M.G., 1954. A method of sampling coarse river-bed material. Eos, Transactions American Geophysical Union 35, 951–956. https://doi.org/10.1029/TR035i006p00951
94. Wolman, M.G., Brush, L.M., 1961. Factors controlling the size and shape of stream channels in coarse noncohesive sands. US Government Printing Office.
95. Xiao, H., Liu, G., Liu, P., Zheng, F., Zhang, J., Hu, F., 2017. Sediment transport capacity of concentrated flows on steep loessial slope with erodible beds. Sci Rep 7, 2350. https://doi.org/10.1038/s41598-017-02565-8
96. Yang, D., Wang, X., Zhang, H., Yin, Z., Su, D., Xu, J., 2021. A Mask R-CNN based particle identification for quantitative shape evaluation of granular materials. Powder Technology 392, 296–305. https://doi.org/10.1016/j.powtec.2021.07.005